Article

Chemistry & Biology

Small-Molecule Disruption of RAD52 Rings as a Mechanism for Precision Medicine in BRCA-Deficient Cancers

Graphical Abstract

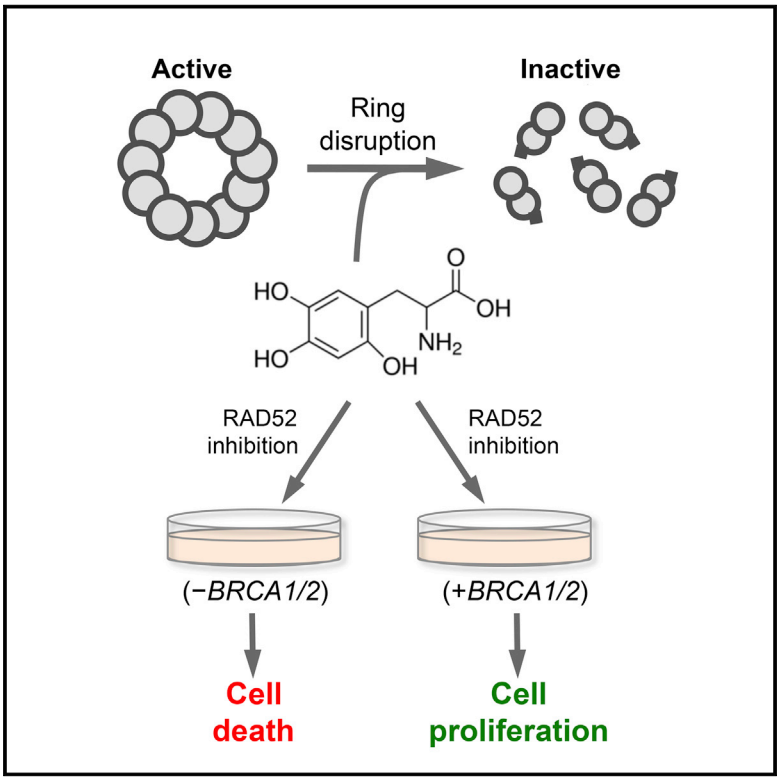

Authors

Gurushankar Chandramouly, Shane McDevitt, Katherine Sullivan, ..., Mark Andrake, Tomasz Skorski, Richard T. Pomerantz

Correspondence

richard.pomerantz@temple.edu

In Brief

Chandramouly et al. show that the small molecule 6-hydroxy-DL-dopa prevents RAD52 from binding to single-strand DNA by disrupting oligomeric ring structures of the protein, and selectively kills BRCA-deficient cell lines and leukemia patient cells by allosterically inactivating RAD52.

Highlights

- Small-molecule inhibition of RAD52 activity in vitro and in vivo
- Small-molecule dimerization of RAD52 undecamer rings
- Small-molecule disruption of RAD52 ring superstructures
- Small-molecule inhibition of RAD52 selectively kills BRCA-deficient cells

Chandramouly et al., 2015, Chemistry & Biology 22, 1491–1504
November 19, 2015
http://dx.doi.org/10.1016/j.chembiol.2015.10.003

Chemistry & Biology
Article

Small-Molecule Disruption of RAD52 Rings as a Mechanism for Precision Medicine in BRCA-Deficient Cancers

Gurushankar Chandramouly,[1,5] Shane McDevitt,[1,5] Katherine Sullivan,[2] Tatiana Kent,[1] Antonio Luz,[3] J. Fraser Glickman,[3] Mark Andrake,[4] Tomasz Skorski,[2] and Richard T. Pomerantz[1,*]
[1]Department of Medical Genetics and Molecular Biochemistry, Fels Institute for Cancer Research, Temple University School of Medicine, Philadelphia, PA 19140, USA
[2]Department of Microbiology and Immunology, Fels Institute for Cancer Research, Temple University School of Medicine, Philadelphia, PA 19140, USA
[3]High-Throughput and Spectroscopy Resource Center, The Rockefeller University, New York, NY 10065, USA
[4]Institute for Cancer Research, Fox Chase Cancer Center, Temple Health, Philadelphia, PA 19111, USA
[5]Co-first author
*Correspondence: richard.pomerantz@temple.edu
http://dx.doi.org/10.1016/j.chembiol.2015.10.003

SUMMARY

Suppression of RAD52 causes synthetic lethality in BRCA-deficient cells. Yet pharmacological inhibition of RAD52, which binds single-strand DNA (ssDNA) and lacks enzymatic activity, has not been demonstrated. Here, we identify the small molecule 6-hydroxy-DL-dopa (6-OH-dopa) as a major allosteric inhibitor of the RAD52 ssDNA binding domain. For example, we find that multiple small molecules bind to and completely transform RAD52 undecamer rings into dimers, which abolishes the ssDNA binding channel observed in crystal structures. 6-OH-Dopa also disrupts RAD52 heptamer and undecamer ring superstructures, and suppresses RAD52 recruitment and recombination activity in cells with negligible effects on other double-strand break repair pathways. Importantly, we show that 6-OH-dopa selectively inhibits the proliferation of BRCA-deficient cancer cells, including those obtained from leukemia patients. Taken together, these data demonstrate small-molecule disruption of RAD52 rings as a promising mechanism for precision medicine in BRCA-deficient cancers.

INTRODUCTION

Homologous recombination (HR) is an essential DNA repair pathway due to its accurate and predominant role in DNA break repair during S phase and G2 (Li and Heyer, 2008; Moynahan and Jasin, 2010; Sung and Klein, 2006). Heritable mutations in HR factors, most notably BRCA1 and BRCA2, cause genome instability and predispose to breast and ovarian cancer (Lok and Powell, 2012; Moynahan and Jasin, 2010). BRCA deficiencies are also observed in a variety of other cancers including lung, prostate, and pancreatic cancers, melanomas, and leukemias (Cramer-Morales et al., 2013; Francis et al., 2010; Mai et al., 2009; Wang et al., 2014). BRCA-deficient-like phenotypes due to spontaneous mutations or defects in HR that are independent of *BRCA1/2* are also commonly observed in cancer cells (Ceccaldi et al., 2015; McCabe et al., 2006; Turner et al., 2004). Because HR-defective cells are impaired in their ability to repair DNA breaks during S phase and G2, DNA damage caused during replication causes severe growth defects in these cells, with little or no effect in normal cells. Thus, drugs that induce DNA damage or further inhibit DNA repair during replication can cause synthetic lethality in BRCA-deficient cells while sparing normal cells (Farmer et al., 2005; McCabe et al., 2006).

The ability to target BRCA-deficient cells for killing has received wide attention due to the potential development of non-toxic drugs for personalized medicine. A notable example includes poly(ADP-ribose) polymerase 1 (PARP-1) inhibitors, which cause replication-dependent DNA breaks and thus preferentially kill BRCA-deficient cells (Farmer et al., 2005; McCabe et al., 2006). Thus far PARP-1 inhibitors, such as the recently approved drug olaparib, have shown promise in the clinic, barring some side effects (Kaufman et al., 2015; Lord and Ashworth, 2012). However, considering that PARP-1 has wide-ranging roles in transcription, translation, telomere maintenance, chromatin, and cellular stress response, in addition to DNA repair, its inhibition inevitably causes a large number of short-term, and possibly long-term, side effects in normal cells (Farmer et al., 2005; Gibson and Kraus, 2012; Ji and Tulin, 2010; Lord and Ashworth, 2012; Thomas and Tulin, 2013). Identifying and characterizing new drug targets that exclusively perform DNA repair as a backup to HR during S phase and G2 will lead to the development of personalized medicine for BRCA-deficient cancer patients with a significantly lower risk of side effects.

Previous studies demonstrated that cells deficient in BRCA1/2 or associated proteins in this pathway (PALB2, RAD51B/C/D, XRCC2/3), combined with a deficiency in recombination factor RAD52, are synthetic lethal (Chun et al., 2013; Feng et al., 2011; Lok et al., 2013; Lok and Powell, 2012). Cells and mice deficient in only RAD52, however, are viable with no apparent phenotypes (Feng et al., 2011; Lok and Powell, 2012; Rijkers et al., 1998). Thus, these studies have revealed a new vulnerability in BRCA-deficient cells which may be exploited to target

these cells for killing. For example, drugs that inhibit RAD52 activity are likely to cause synthetic lethality in BRCA-deficient cells in a manner similar to PARP-1 inhibitors, but potentially have no side effects (Lok and Powell, 2012).

Much of our knowledge of how RAD52 functions has been derived from studies in the yeast model *Saccharomyces cerevisiae*. For example, yeast Rad52 plays a major role in HR by facilitating loading of Rad51 recombinase onto RPA-coated single-stranded DNA (ssDNA), which is necessary for strand invasion and subsequent steps of HR (Krogh and Symington, 2004; Liu and Heyer, 2011). This function is consistent with the ability of Rad52 to bind ssDNA, RPA, and Rad51. Since Rad52 plays a prominent role in Rad51 loading, yeasts deficient in Rad52 are impaired in HR and highly sensitive to genotoxic agents (Krogh and Symington, 2004). Rad52 in yeast and higher eukaryotes is also essential for the repair of double-strand breaks (DSBs) by single-strand annealing (SSA) (Kagawa et al., 2002; Krogh and Symington, 2004; Singleton et al., 2002). In this pathway, RAD52 uses sequence microhomology along ssDNA exposed by nuclease processing of DSBs to recombine broken DNA, which results in chromosomal deletions (Krogh and Symington, 2004).

In contrast to yeast, RAD51 loading in mammalian cells is primarily performed by the BRCA pathway, whereas RAD52 appears to play a backup role (Feng et al., 2011; Lok et al., 2013; Lok and Powell, 2012). For example, previous studies have shown that suppression of RAD52 expression has little or no effect on HR in BRCA-proficient cells (Feng et al., 2011; Lok et al., 2013). Yet suppression of RAD52 in BRCA-deficient cells further reduces HR and RAD51 loading, and causes synthetic lethality (Feng et al., 2011; Lok et al., 2013). Hence, these studies suggest that RAD52 might promote the survival of BRCA-deficient cells by facilitating RAD51-dependent HR. Considering that RAD52 is also essential for SSA, which functions during S phase, its annealing activity probably also contributes to the survival of BRCA-defective cells. Although the exact mechanism by which RAD52 promotes the survival of BRCA-deficient cells remains unclear, a recent report showed that its ssDNA binding activity is essential for this role (Cramer-Morales et al., 2013). Altogether, these studies indicate that small-molecule inhibitors of the RAD52 ssDNA binding domain are likely to target BRCA-deficient cells for killing.

The crystal structure of the RAD52 ssDNA binding domain, for example residues 1–209, has been solved by two groups (Kagawa et al., 2002; Singleton et al., 2002). Remarkably, 11 monomers form an undecamer ring with a positively charged channel around its outer surface that likely interacts with ssDNA (Kagawa et al., 2002; Singleton et al., 2002). Although DNA binding motifs are traditionally considered to be "undruggable," small-molecule disruption of protein complexes is a promising strategy for inhibiting multi-subunit DNA binding proteins (Scheuermann et al., 2013). Here, we identify and characterize a small-molecule allosteric inhibitor of RAD52 that disrupts ring structures of the protein and selectively impairs the growth of BRCA-deficient cancer cells.

RESULTS

Identification of RAD52 Small-Molecule Inhibitors

Since recent studies have shown that the proliferation of BRCA-deficient cells depends on RAD52 ssDNA binding activity (Cramer-Morales et al., 2013), we set out to identify inhibitors of the ssDNA binding domain. A fluorescence polarization (FP) assay that detects RAD52 ssDNA binding was optimized and adapted for high-throughput screening as follows (Figure 1A, left). A 29-nt ssDNA probe conjugated with fluorescein (FAM) was incubated with increasing concentrations of wild-type (WT) RAD52, which forms a 323-kDa heptamer ring and higher-order heptamer ring superstructures (Lloyd et al., 2002; Stasiak et al., 2000; Van Dyck et al., 1998; Van Dyck et al., 2001). After 30 min FP was determined, which is inversely proportional to the rotation rate of the ssDNA probe (Figure 1A, middle). RAD52 binding caused an increase in polarization due to slowed rotation of the ssDNA probe. FP reactions, with and without RAD52, performed in 384-well high-throughput format using a liquid handler resulted in a high Z' score of 0.82, demonstrating that the assay was consistent and suitable for high-throughput screening (Figure 1A, right).

We screened a diverse set of 18,304 drug-like compounds and the Sigma Lopac collection of 1,280 pharmacologically active compounds, and identified ten small molecules that consistently inhibited RAD52 ssDNA binding by more than 60% and exhibited a relatively low IC_{50} (≤ 5 μM) (Figures 1B and 1C). The small molecules were confirmed by high-performance liquid chromatography-mass spectrophotometry or newly purchased. Small-molecule inhibition of RAD52 ssDNA binding was confirmed using an orthogonal electrophoresis mobility shift assay (EMSA) (Figure 1D). Similarly to previous studies, RAD52 shifted the ssDNA probe to the wells of the polyacrylamide gel due to its 323-kDa heptamer ring conformation and tendency to form higher-order heptamer ring superstructures (Benson et al., 1998; Lloyd et al., 2002; Van Dyck et al., 1998). As a control, we showed that these large RAD52-ssDNA complexes were resolved in an agarose gel as in previous studies (Figure S1) (Benson et al., 1998). Select compounds that inhibited RAD52 by more than 70% were further analyzed in cells.

Small-Molecule Inhibition of RAD52 Activity in Cells

We examined the effects of select small molecules on SSA, which is one of the main activities of RAD52 (Kagawa et al., 2002; Krogh and Symington, 2004; Singleton et al., 2002). To measure SSA, a previously characterized GFP reporter system was used that detects activation of GFP expression as a result of SSA repair of an I-SceI-induced DSB (Gunn et al., 2011; Gunn and Stark, 2012). As a control, we demonstrated that suppression of RAD52 via siRNA inhibited SSA as expected (Figure 2A). Surprisingly, only one of the small molecules, 6-hydroxy-DL-dopa (6-OH-dopa), a precursor of the catecholaminergic neurotoxin 6-hydroxydopamine, consistently inhibited SSA (Figure 2B). The remaining compounds showed either no effect, slight inhibition, or stimulation of SSA, which was probably due to off-target effects. As a control, we showed that the effect of 6-OH-dopa was dose dependent (Figure 2C). Inhibition of SSA by 6-OH-dopa was additionally confirmed in vitro (Figure S1), and was dependent on RAD52 expression (Figure S2). We also confirmed that 6-OH-dopa does not interact with ssDNA (Figure S1). Importantly, we found that small molecules similar in structure to 6-OH-dopa, including L-DOPS which is in the same catechol chemical class, failed to inhibit SSA (Figure 2D) and RAD52 ssDNA binding (Figure S1). Thus, these data indicate that a specific interaction between

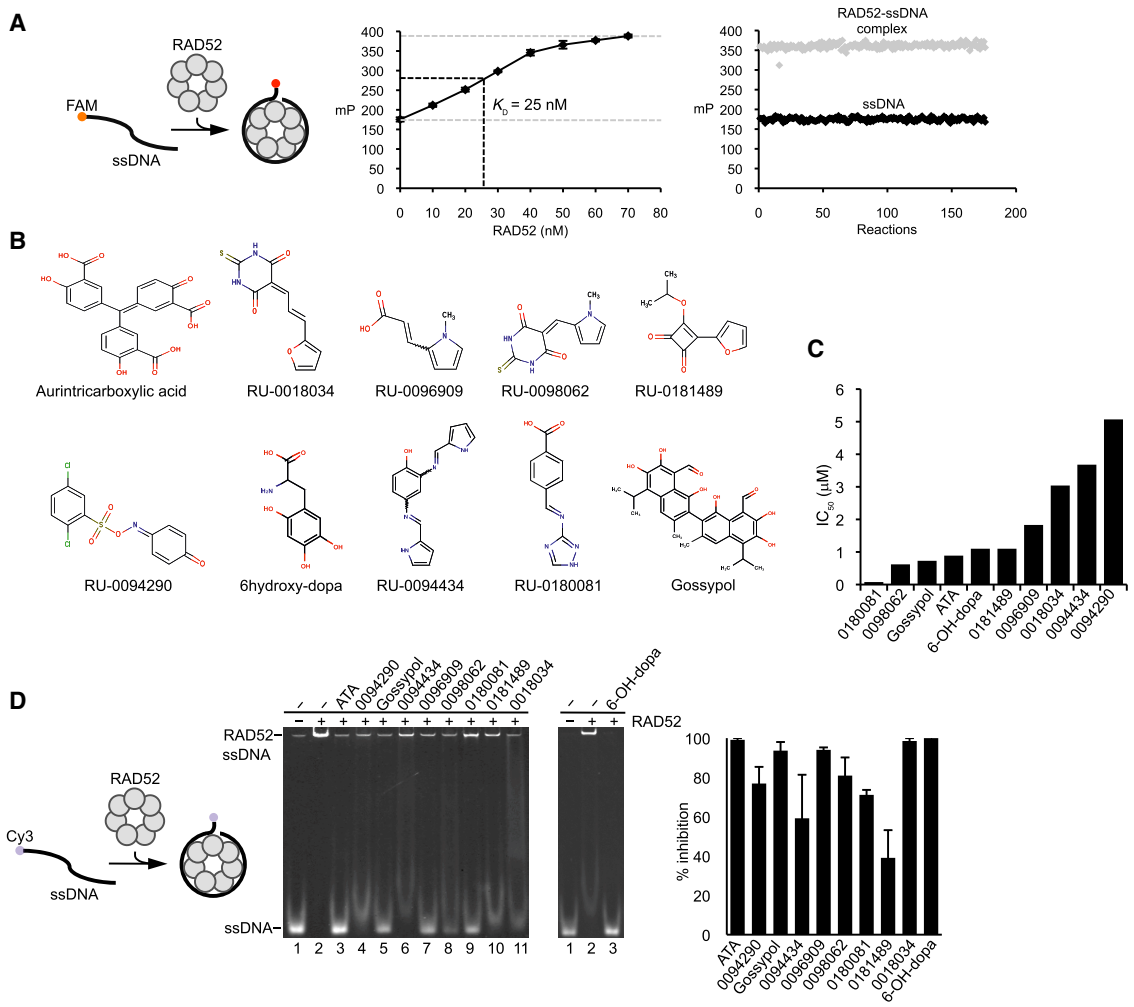

Figure 1. Identification of RAD52 Inhibitors by High-Throughput Screening

(A) Schematic of fluorescence polarization (FP) assay (left). Plot showing RAD52 binding to ssDNA probe. K_D = 25 nM. Data shown as average ± SD from four independent experiments (middle). Plot showing 176 high-signal (RAD52 with ssDNA probe) and 176 low-signal (ssDNA probe only) FP control reactions performed in 384-well high-throughput format. Z' factor = 0.82. mP, millipolarization.

(B) Structures of select identified RAD52 inhibitors.

(C) Plot showing IC_{50} for RAD52 inhibitors.

(D) Schematic of electrophoresis mobility shift assay (EMSA) (left). Non-denaturing gel of EMSA showing inhibition of RAD52 by 60 μM of indicated small molecules (middle panels). Plot of EMSA data shown as percent inhibition of RAD52. Data shown as average ± SD from three independent experiments (right).

6-OH-dopa and RAD52 is responsible for the observed inhibitory effects in vitro and in vivo.

We further examined the specificity of 6-OH-dopa for RAD52 in cells by investigating its effects on other DSB repair pathways. First, we tested whether 6-OH-dopa inhibits HR, which shares the same upstream DNA damage response and resection pathways as SSA. Since HR functions mostly independently of RAD52 in BRCA-proficient cells, we anticipated that inhibition of RAD52 would have little effect on HR (Feng et al., 2011; Lok et al., 2013). Indeed, using a previously characterized HR GFP reporter (Gunn et al., 2011; Gunn and Stark, 2012), we found that 6-OH-dopa treatment resulted in little or no reduction in HR (Figure 2E), and had no effect on HR when RAD52 was suppressed (Figure S2). Thus, these data are consistent with the ability of 6-OH-dopa to inhibit RAD52 with a considerable amount of specificity. In support of this, we found that 6-OH-dopa had little or no effect on RAD51 (IC_{50} not determined) compared with RAD52 (IC_{50} = 1.1 μM) in vitro (Figure 2F). 6-OH-Dopa also had a significantly higher IC_{50} (> 10 μM) for *S. cerevisiae* RAD59, which shares 31.5% sequence identity with human RAD52 and performs a similar SSA activity (Figures 2F and S3) (Krogh and Symington, 2004; Petukhova et al., 1999; Wu et al., 2006). We note that the small molecules that inhibited HR (RU-0180081, RU-0096909) showed stimulation of SSA, which is expected, based on the ability of HR to suppress SSA (Figures 2E and 2B) (Stark et al., 2004; Tutt et al., 2001). To further analyze the specificity of 6-OH-dopa for RAD52 in cells, we tested its effect on non-homologous end joining (NHEJ). Using another previously characterized GFP reporter (Gunn et al., 2011; Gunn and Stark, 2012), we found that 6-OH-dopa only

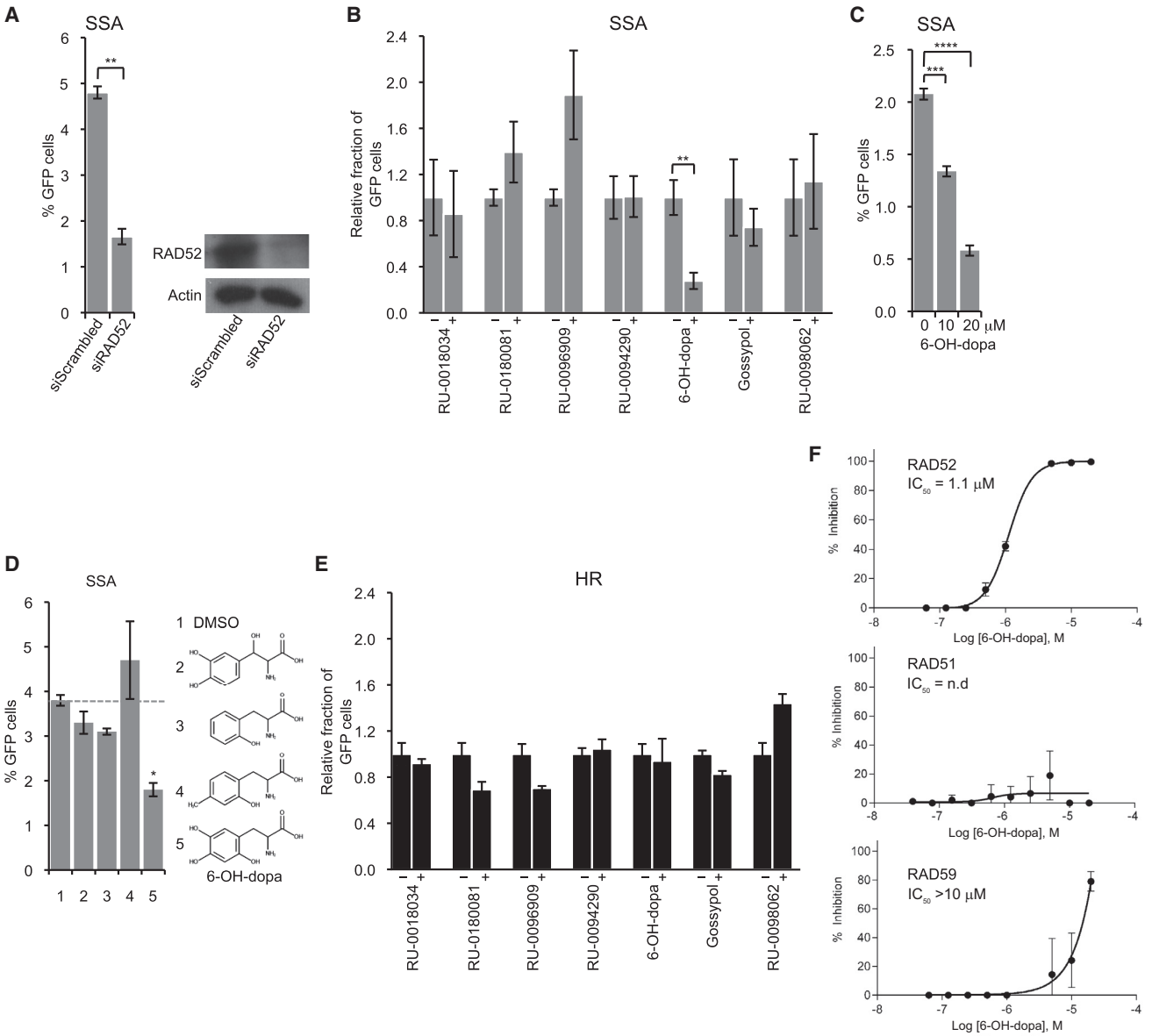

(legend on next page)

slightly inhibited NHEJ (Figure 2G). Considering that HR and NHEJ each require a host of proteins involved in nucleic acid processing, signaling, and protein post-translational modification, the ability of 6-OH-dopa to selectively inhibit SSA in cells demonstrates a considerable amount of specificity of the small molecule for RAD52 (Ciccia and Elledge, 2010; Deriano and Roth, 2013; Moynahan and Jasin, 2010). Thus, although 6-OH-dopa is a catechol and has the potential to interfere with some assays non-specifically, the exhaustive in vitro and cell-based data presented herein show that its mechanism on RAD52 is specific.

We further examined the ability of 6-OH-dopa to inhibit RAD52 activity in cells by testing its effects on RAD52 foci formation at DNA damage caused by cisplatin and ionizing radiation (Figure 3). eGFP-RAD52 was stably expressed in BCR-ABL transformed murine hematopoietic 32Dcl3 cells, which are known to be deficient in BRCA1 (Cramer-Morales et al., 2013; Podszywalow-Bartnicka et al., 2014). Previous studies have demonstrated that eGFP-RAD52 is functional in cells (Essers et al., 2002; Feng et al., 2011), and we found that the purified protein acts like WT RAD52 in vitro (Figure S1). The eGFP-RAD52-expressing cells were incubated with DMSO or 6-OH-dopa and further treated with cisplatin, which causes intra- and inter-strand cross-links that arrest replication forks. Consistent with the ability of the small molecule to inhibit RAD52 ssDNA binding, 6-OH-dopa suppressed eGFP-RAD52 foci formation in a dose-dependent manner (Figures 3A and S4). We further investigated the effect of 6-OH-dopa on eGFP-RAD52 foci in HEK293T cells exposed to ionizing radiation. The small molecule again decreased the number of eGFP-RAD52 foci in a dose-dependent manner (Figures 3B and S4). 6-OH-Dopa also inhibited eGFP-RAD52 foci in MDA-MB-436 cells complemented with BRCA1 following exposure to ionizing radiation (Figures 3C and S4). Together, these results demonstrate that 6-OH-dopa effectively inhibits RAD52 ssDNA binding in vivo.

Small-Molecule Dissociation of RAD52-ssDNA Complexes

We next considered whether 6-OH-dopa was capable of dissociating pre-formed RAD52-ssDNA complexes. Given that RAD52 bound tightly to ssDNA (K_D = 25 nM; Figure 1A), we anticipated that RAD52-ssDNA complexes would be resistant to 6-OH-dopa treatment. To test this, RAD52-ssDNA complexes were formed and allowed to reach equilibrium after 30 min of incubation. 6-OH-Dopa was then added and FP was measured 2 min later. Remarkably, the small molecule fully dissociated RAD52-ssDNA complexes as indicated by a reduction in millipolarization levels nearly identical to those observed for the DNA control (Figure 4A). 6-OH-Dopa dissociation of RAD52-ssDNA complexes was also observed by EMSA (Figure 4B).

The ability of the small molecule to rapidly dissociate RAD52-ssDNA complexes suggested that it might act as a non-competitive inhibitor. To test this, we investigated whether the inhibitory activity of the small molecule was diminished by simultaneously adding a large of excess of ssDNA substrate. Strikingly, the small molecule continued to inhibit RAD52 in the presence of a ~100-fold excess of the ssDNA substrate (Figure 4C). Hence, these data suggest that the small molecule binds to a different site than the ssDNA binding channel, and thus acts a non-competitive inhibitor.

Small-Molecule Disruption of RAD52 Rings

To gain more insight into the mechanism of 6-OH-dopa action, we examined its interaction with RAD52. Since the small molecule inhibits RAD52 ssDNA binding, we envisaged that it acted on the ssDNA binding domain (residues 1–209; RAD52 1–209). X-Ray crystallographic studies demonstrate that the ssDNA binding domain forms an undecamer ring with a large central channel (Kagawa et al., 2002; Singleton et al., 2002). The 11 subunits form a symmetrical pinwheel-like conformation with a positively charged channel circling the outer surface that likely interacts with ssDNA (Kagawa et al., 2002; Singleton et al., 2002). We found that the small molecule inhibited RAD52 1–209 with an IC_{50} (1.6 μM) comparable with that of WT RAD52 (1.1 μM), indicating that it interacts with the ssDNA binding domain (Figures 5A and 5B). Isothermal titration calorimetry (ITC) confirmed that 6-OH-dopa interacts with the ssDNA binding domain with a K_D of 17.7 μM (Figure 5C). Unexpectedly, these data suggested a stoichiometry of 5.04 small molecules per RAD52 1–209 ring (Figure 5C). This suggests the possibility that one small molecule binds to every other subunit around the ring (Figure 5C), which is plausible based on the slightly different orientation of subunits (Kagawa et al., 2002; Singleton et al., 2002). Alternatively, the small molecule may bind at the interface of every other subunit pair, which would also account for approximately five binding sites.

Considering that 6-OH-dopa may inhibit RAD52 by acting at multiple subunit interfaces, we wondered whether the small

Figure 2. 6-OH-dopa Selectively Inhibits RAD52-Mediated Recombination in Vivo

(A) Plot showing SSA in U20S cells treated with scrambled and RAD52 siRNA. Data represent mean ± SEM from triplicates. **p = 0.00036, two-tailed Student's t test (left). Western blots of protein extracts from U20S cells treated with scrambled and RAD52 siRNA (right).

(B) Plot showing SSA in U20S cells following treatment with 5 μM of the indicated small molecules. Data represent mean ± SEM from three separate experiments with triplicates in each experiment. **p = 0.00154, two-tailed Student's t test.

(C) Plot showing SSA in U20S cells following treatment with 0, 10, and 20 μM of 6-OH-dopa. Data represent mean ± SEM from triplicates. ***p = 0.00039, ****p = 0.00009, two-tailed Student's t test.

(D) Plot showing SSA in U20S cells following treatment with 5 μM of the indicated small molecules. 2, L-DOPS; 3, DL-o-tyrosine; 4, β-(2-hydroxy-4-methylphenyl) alanine; 5, 6-OH-dopa. Data represent mean ± SEM from triplicates. *p = 0.00175, two-tailed Student's t test.

(E) Plot showing HR in U20S cells following treatment with 5 μM of the indicated small molecules. Data represent mean ± SEM from three separate experiments with triplicates in each experiment.

(F) Plots showing percent inhibition of indicated protein as a function of 6-OH-dopa concentration. Data shown as average ± SEM from three independent experiments.

(G) Plot showing NHEJ in U20S cells following treatment with or without 5 μM of 6-OH-dopa. Data represent average ± SEM from two separate experiments with triplicates in each experiment.

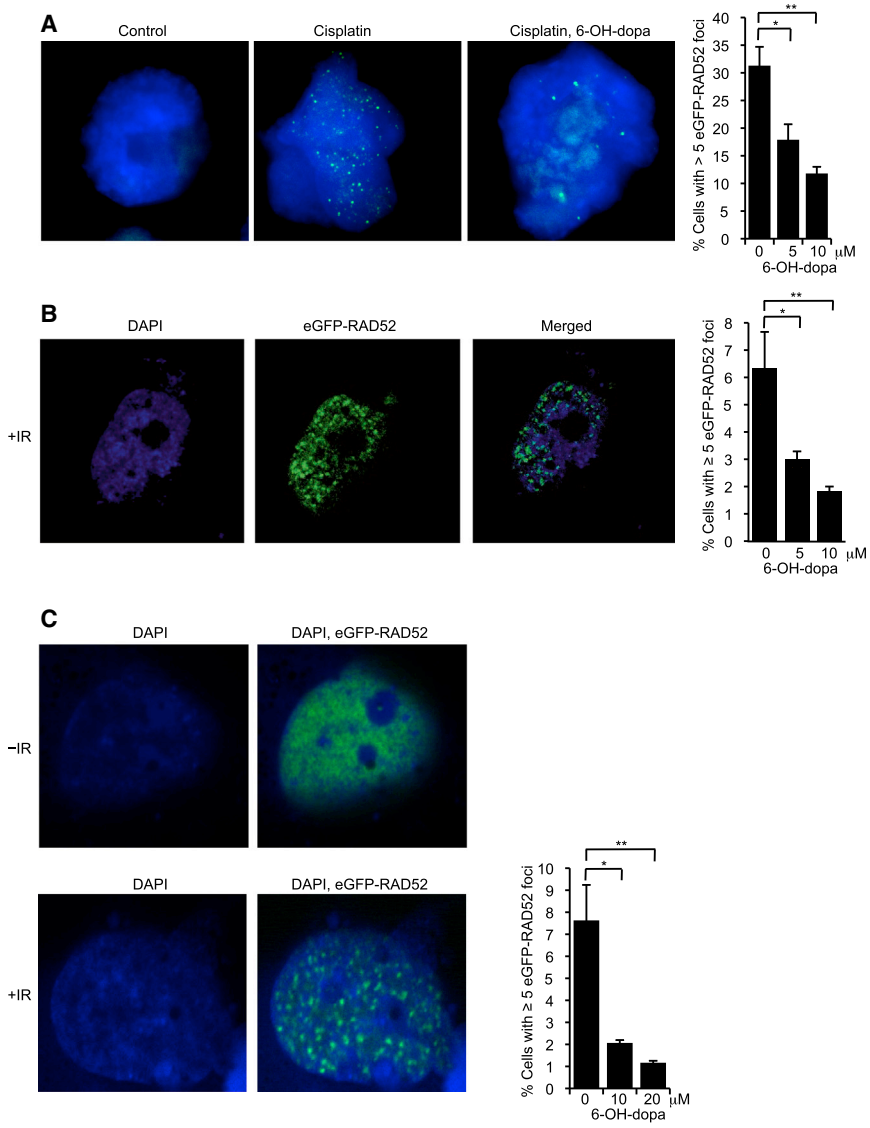

Figure 3. 6-OH-dopa Inhibits RAD52 Foci Formation

(A) Cells stably expressing eGFP-RAD52 were exposed to cisplatin and 6-OH-dopa. Representative images of nuclei counterstained with DAPI (blue) and eGFP-RAD52 (green) (left). Plot showing quantification of cells with eGFP-RAD52 foci following treatment with cisplatin and 6-OH-dopa (right). Data represent mean ± SEM from triplicates. *p = 0.01, **p = 0.007, two-tailed Student's t test.

(B) Representative fluorescent images of HEK293T cells visualizing DAPI stain (blue) and EGFP fluorescence (green) following treatment with ionizing radiation (IR) (left). Plot showing percent HEK293T cells with ≥5 eGFP-RAD52 foci following treatment with IR and 6-OH-dopa (right). Data shown as average ± SEM from three independent experiments. *p = 0.05, **p = 0.03, two-tailed Student's t test.

(C) Representative fluorescent images of MDA-MB-436 BRCA1 complemented cells visualizing DAPI stain (blue) and EGFP RAD52 (green) following treatment with or without IR (left). Plot showing percent MDA-MB-436 BRCA1 complemented cells with ≥5 eGFP-RAD52 foci following treatment with IR and 6-OH-dopa (right). Data shown as average ± SEM from three independent experiments. *p = 0.03, **p = 0.02, two-tailed Student's t test.

molecule altered the structure or composition of the RAD52 1–209 undecamer ring. To test this, we analyzed the mobility of RAD52 1–209 in a native gel following incubation with increasing amounts of the small molecule. Remarkably, 6-OH-dopa enabled the protein to enter the gel, which appeared as multiple discrete bands, the smallest of which was in the range of ~50–100 kDa (Figure 5D, left). Western blot analysis of RAD52 1–209 following native gel electrophoresis confirmed the identity of the bands as RAD52 1–209 (Figure 5D, right). Together, these results indicate that 6-OH-dopa dissociates RAD52 complexes. As a control, we showed that a structurally similar small molecule, DL-o-tyrosine, which failed to inhibit RAD52 (Figure S1), had no effect on RAD52 1–209 composition (Figure S1). We also showed that another potent inhibitor of RAD52 1–209 (RU-0098062; Figures 1B–1D) had no effect on the composition of the protein (Figure S1). Thus, these results clearly show that a specific interaction between 6-OH-dopa and the ssDNA binding domain facilitates dissociation of RAD52 complexes.

Light scattering was used to confirm small-molecule dissociation of RAD52 complexes and to determine the size of the resulting protein species. First, light scattering was performed under high salt conditions, similar to the reactions resolved in native gels. In the absence of the small molecule, the molecular weight of RAD52 1–209 was ~439 kDa, which likely includes a mixture of single, double, and triple undecamer rings (Figure 5E, left). The addition of 6-OH-dopa, however, produced a discrete 48.3-kDa species (Figure 5E, middle) that was not observed in the buffer or small-molecule controls (Figure S5). We note that the 439-kDa peak slightly increased to 595.6 kDa, which may be due to some precipitation of RAD52 1–209 by 6-OH-dopa. Considering that 48.3 kDa is nearly identical in mass to the sum of two monomers of RAD52 1–209 (48 kDa), these data demonstrate that the small molecule dissociates the undecamer ring into dimers (Figure 5E, right). To confirm this result, we repeated the light-scattering experiment under low salt conditions, which reduce hydrophobic interactions such as those that promote RAD52 superstructures. Indeed, under low salt conditions RAD52 1–209 was mostly detected at 270 kDa, which closely corresponds to its undecamer form (263 kDa) (Figure 5F, left). Addition of the small molecule again produced a 48.3-kDa species (Figure 5F, middle) that was not observed in the buffer or 6-OH-dopa controls (Figure S5). Remarkably, under these conditions, 100% of the undecamers (270 kDa) were converted into dimers (48.3 kDa), demonstrating that the small molecule is

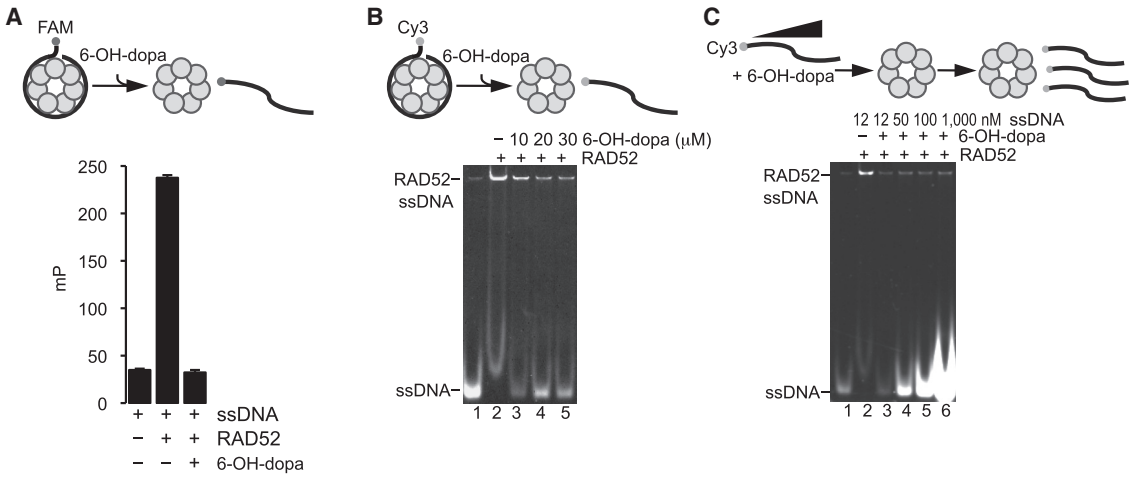

Figure 4. 6-OH-dopa Dissociates RAD52-ssDNA Complexes and Acts as a Non-competitive Inhibitor

(A) Schematic of FP assay (top). Plot showing dissociation of RAD52-ssDNA complexes by 30 μM 6-OH-dopa (bottom). Data shown as average ± SD from three independent experiments. mP, millipolarization.

(B) Schematic of EMSA (top). Non-denaturing gel showing dissociation of RAD52-ssDNA complexes by 30 μM 6-OH-dopa (bottom).

(C) Schematic of EMSA (top). Non-denaturing gel showing 6-OH-dopa (25 μM) inhibition of RAD52 in the presence of excess of Cy3-ssDNA substrate (bottom).

more active when hydrophobic interactions are suppressed by low salt (Figure 5F, right).

Although electron microscopy studies demonstrate that RAD52 WT forms heptamer rings and large heptamer ring superstructures (Stasiak et al., 2000; Van Dyck et al., 1998, 2001), the atomic structure of full-length RAD52 has not been solved. Thus, it remains unknown whether the RAD52 WT heptamer ring possesses an ssDNA binding channel like that observed in the RAD52 1–209 undecamer ring. However, considering that 6-OH-dopa exhibits a comparable IC_{50} for RAD52 WT (1.1 μM) and RAD52 1–209 (1.6 μM), the ssDNA binding domain is likely to have a similar conformation in the heptamer and undecamer forms. We therefore examined whether 6-OH-dopa had similar effects on the composition of RAD52 WT heptamer rings. Indeed, the small molecule enabled RAD52 WT to enter a native gel as discrete higher molecular weight complexes in a similar manner as observed for RAD52 1–209 (compare Figures 5G and 5D). The lower molecular weight complex appeared slightly larger than 670 kDa, which corresponds to a double heptamer and is consistent with previous gel filtration studies (Figure 5G) (Lloyd et al., 2005). The higher molecular weight complexes likely represent heptamer ring superstructures (Figure 5G). In contrast to the results obtained with RAD52 1–209, 6-OH-dopa failed to produce smaller molecular weight complexes from RAD52 WT (compare Figures 5G and 5D). To more accurately determine the size of RAD52 WT complexes following incubation with 6-OH-dopa, we analyzed the protein by gel filtration. Similarly to previous studies, the molecular weight of RAD52 WT in the absence of 6-OH-dopa was around 670 kDa, which corresponds to a double heptamer ring (Figure 5H, black line) (Lloyd et al., 2005). Notably, only a small fraction of the loaded protein entered the column, which we attribute to the tendency of RAD52 WT to form large superstructures that are excluded from the column. Consistent with this interpretation, most of RAD52 WT failed to enter the native gel in the absence of the small molecule (Figure 5G). Similar to the results obtained from native gel analysis, the small molecule enabled a significantly higher concentration of RAD52 WT to enter the column as multiple discrete higher molecular weight complexes (Figure 5H, red line). The smaller peak corresponds to a double heptamer, whereas the larger peak migrated as larger superstructures, probably composed of three to four heptamer rings (Figure 5H, red line). Taken together, these experiments demonstrate that 6-OH-dopa disrupts RAD52 heptamer and undecamer ring superstructures, and further dissociates undecamer rings into dimers.

Selective Killing of BRCA-Deficient Cells by Small-Molecule Inhibition of RAD52

Since RAD52 ssDNA binding activity has been shown to be essential for the survival of BRCA-deficient cells (Cramer-Morales et al., 2013), we examined whether 6-OH-dopa selectively reduces the viability of cells harboring mutations in *BRCA1/2*. As a control, we tested whether suppression of RAD52 reduced the viability of the BRCA1-deficient triple-negative breast cancer cell line MDA-MB-436. Similar to previous studies using other BRCA1-deficient cells (Lok et al., 2013), we found that suppression of RAD52 via small interfering RNA (siRNA) (Figure S2) resulted in reduced viability after a short 3-day time course (Figure 6A). In contrast, suppression of RAD52 caused a slight increase in the viability of the same cell line complemented with WT *BRCA1* (Figure 6A); scrambled siRNA had negligible effects on viability (Figure 6A). As a further control, we showed that olaparib selectively reduced the viability of the *BRCA1*-mutated cells, as expected (Figure 6A). Remarkably, 6-OH-dopa treatment resulted in a nearly identical reduction in viability of the BRCA1-deficient cells (Figure 6A). 6-OH-Dopa also selectively halted the proliferation of the Chinese hamster cell line VC8 (Figure 6B) and the pancreatic cancer cell line CAPAN-1 (Figure 6C), which are both defective in BRCA2 due to truncation mutations. Similar growth defects were observed following olaparib treatment (Figures 6B and 6C), demonstrating that the

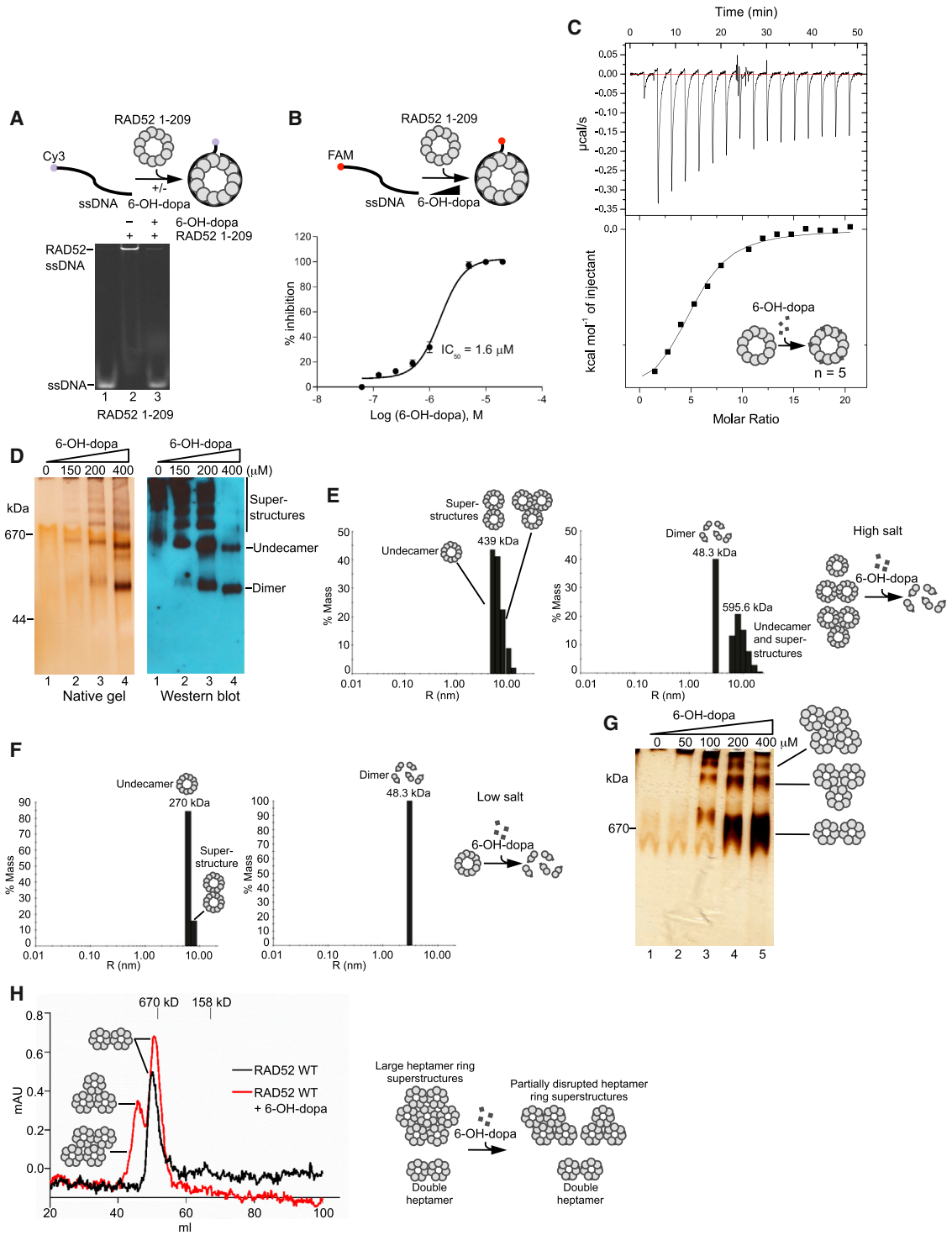

Figure 5. 6-OH-dopa Targets the RAD52 ssDNA Binding Domain and Disrupts RAD52 Rings

(A) Schematic of EMSA (top). Non-denaturing gel of EMSA showing 6-OH-dopa inhibition of RAD52 1–209 (bottom).

(B) Schematic of FP assay (top). Plot showing percent inhibition of RAD52 1–209 ssDNA binding as a function of 6-OH-dopa concentration. IC_{50} = 1.6 μM. Data shown as average ± SD from three independent experiments (bottom).

(C) Plot of isothermal titration calorimetry (ITC) data showing 6-OH-dopa interaction with RAD52 1–209. K_D = 17.8 μM, n = 5. Model of 6-OH-dopa binding to RAD52 1–209 (inset).

(D) Silver-stained non-denaturing gel of RAD52 1–209 following incubation with 6-OH-dopa (left). Western blot of non-denaturing gel of RAD52 1–209 following incubation with 6-OH-dopa (right).

(legend continued on next page)

ability of 6-OH-dopa to selectively inhibit the proliferation of BRCA-deficient cells is comparable with olaparib. 6-OH-Dopa also selectively reduced the viability of the BRCA1-deficient triple-negative breast cancer cell line HCC1937 (Figure 6D).

The ability of 6-OH-dopa to target BRCA-deficient cells was further examined in clonogenic survival assays. We observed that 6-OH-dopa inhibited the survival of BRCA-deficient cell lines, while having little or no effect on BRCA-proficient cells at the given doses (Figures 6E and 6F). Considering that previous studies have revealed BRCA deficiencies in acute myeloid leukemia (AML) and chronic myelogenous leukemia (CML) (Cramer-Morales et al., 2013; Podszywalow-Bartnicka et al., 2014), we examined the ability of 6-OH-dopa to halt the growth of AML and CML patient cells that were previously identified as expressing low levels of BRCA1/2 (Figure S6) (Cramer-Morales et al., 2013; Podszywalow-Bartnicka et al., 2014). Remarkably, treatment with 6-OH-dopa or olaparib resulted in a similar reduction in colony formation by BRCA-deficient AML patient cells with little effects on AML patient cells expressing normal levels of BRCA1/2 (Figure 6G). We also observed a significant reduction in the survival of BRCA1-deficient CML patient cells treated with 6-OH-dopa (Figure 6H). To rule out the possibility that the selective killing of BRCA-deficient cells was due to an off-target effect, we examined the effect of 6-OH-dopa on the viability of cells deficient in both the BRCA pathway and RAD52. For example, in the event that 6-OH-dopa selectively halted the proliferation of BRCA-deficient cells by inhibiting a target other than RAD52, the small molecule would still substantially reduce the viability of BRCA-deficient cells that lacked RAD52. The small molecule, however, lost its ability to significantly reduce the viability of BRCA1-deficient cells when RAD52 expression was suppressed (Figure 6I) (Figure S2). Thus, these data indicate that the selective growth inhibition of BRCA-deficient cells by 6-OH-dopa results from its ability to inactivate RAD52.

Small-Molecule Inhibition of RAD52 Causes DNA Damage and Apoptosis in BRCA-Deficient Cells

Since RAD52 is recruited to DNA breaks caused by replicative stress (Figure 3A) (Lisby et al., 2001; Wray et al., 2008), the reduced viability of BRCA-deficient cells due to RAD52 inhibition is likely caused by insufficient repair of DNA breaks caused by replication stress. Consistent with this, we observed that 6-OH-dopa treatment resulted in a substantial increase in DNA damage indicated by γH2AX foci, which was significantly more pronounced in BRCA-deficient cells (Figure 6J). We also found that 6-OH-dopa specifically increased apoptosis in BRCA-deficient cells, indicated by annexin V staining (Figure 6K). Taken together, our data indicate that in BRCA-deficient cells 6-OH-dopa inactivation of RAD52 causes cell death due to insufficient repair of DNA breaks caused by regular replicative stress (Figure 7A, right). In contrast, 6-OH-dopa inactivation of RAD52 in BRCA-proficient cells has little or no effect on cell proliferation due to efficient HR repair of replication forks by the primary BRCA pathway (Figure 7A, left).

DISCUSSION

Although previous genetic studies have identified RAD52 as a potential drug target for personalized medicine in BRCA-deficient cancers (Feng et al., 2011; Lok et al., 2013), it remained unknown whether RAD52 could be inactivated by a small molecule, which is a necessary step toward therapeutic development. Here, we identify and characterize 6-OH-dopa as a major allosteric inhibitor of RAD52 that selectively halts the growth of BRCA-deficient cancer cells including those obtained from AML and CML patients. Our findings validate RAD52 as a therapeutic target for precision medicine in BRCA-deficient cancers and showcase a novel allosteric mechanism of inhibition.

Although we initially identified multiple inhibitors of RAD52 in vitro, only 6-OH-dopa consistently inhibited SSA in cells while having minimal effects on HR and NHEJ. Considering that HR and NHEJ each require a host of proteins involved in nucleic acid processing, signaling, and post-translational modifications, these data show that 6-OH-dopa exhibits a considerable amount of specificity for RAD52 in cells. Consistent with this, 6-OH-dopa had no effect on RAD51, which forms a similar heptamer ring structure with nearly identical dimensions as RAD52 (Shin et al., 2003). Intriguingly, this characteristic ring shape is common among replication and repair proteins including the prototypical RecA recombinase (Kagawa et al., 2002; Patel and Picha, 2000; Shin et al., 2003; Singleton et al., 2002; Stasiak et al., 2000; Yu and Egelman, 1997). 6-OH-dopa, however, had very little effect on RecA (Figure S1) and exhibited a 10-fold higher IC_{50} for yeast Rad59, which shares 31.5% sequence identity with RAD52. Thus, the small molecule also showed a considerable amount of specificity for RAD52 in vitro. Importantly, 6-OH-dopa inhibited RAD52 foci in multiple cell lines, which unequivocally demonstrates its ability to inactivate RAD52 in vivo. Thus, although 6-OH-dopa is a catechol and has the potential to interfere with some assays non-specifically, the in vitro and cell data presented herein show that its mechanism on RAD52 is specific.

We discovered an unprecedented allosteric mechanism whereby multiple small molecules bind to RAD52 undecamer rings and promote their dissociation into dimers. To our knowledge, such a dramatic molecular transformation induced by a small molecule has never been reported. Considering that the putative ssDNA binding channel observed in crystal structures is constructed from all 11 subunits and encircles the entire undecamer ring (Kagawa et al., 2002; Singleton et al., 2002), small-molecule dissociation of the ring is certain to abolish the ssDNA binding channel. Since a different potent inhibitor of RAD52 (RU-0098062) failed to dissociate the undecamer, the allosteric

(E) Plots showing light-scattering data of RAD52 1–209 following incubation with (right) and without (middle) 6-OH-dopa with 1 M NaCl. Model of 6-OH-dopa action on RAD52 1–209 with high salt (right).

(F) Plots showing light-scattering data of RAD52 1–209 following incubation with (middle) and without (left) 6-OH-dopa with 0.15 M NaCl. Model of 6-OH-dopa action on RAD52 1–209 with low salt (right).

(G) Silver-stained non-denaturing gel of RAD52 WT following incubation with 6-OH-dopa (left).

(H) Gel-filtration profiles of RAD52 WT following incubation with (red line) and without (black line) 6-OH-dopa (left). Model of 6-OH-dopa action on RAD52 WT (right).

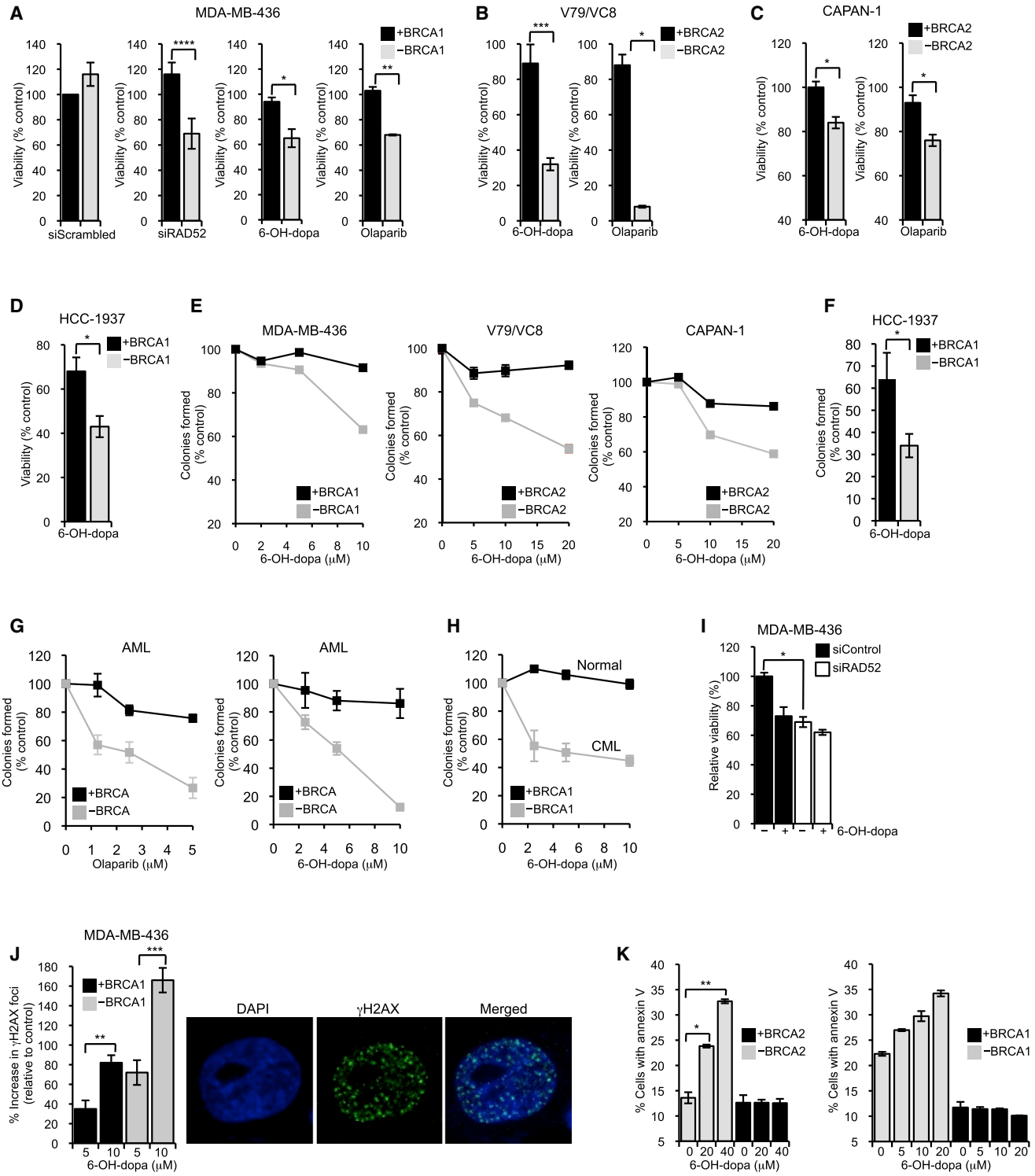

Figure 6. 6-OH-dopa Selectively Inhibits the Growth of BRCA-Deficient Cells

(A–D) Plots showing relative viability of BRCA proficient (black) and deficient (gray) cells following treatment with 20 μM (A), 75 μM (B), 10 μM (C), and 5 μM (D) 6-OH-dopa, 20 μM olaparib (C), or indicated siRNA. Data shown as average ± SEM from triplicates. Two-tailed Student's t test: (A) ****p = 0.0008, *p = 0.02, **p = 0.005; (B) ***p = 0.0002, *p = 0.03; (C) *p = 0.01, *p = 0.01; (D) *p = 0.05.

(E–H) Plots showing clonogenic survival of indicated BRCA-proficient and -deficient cells following treatments with 6-OH-dopa or olaparib. Data shown as average ± SEM from three independent experiments. Data points in (G) and (H) represent three different patient cells pooled together. In (F) *p = 0.03, two-tailed Student's t test.

(legend continued on next page)

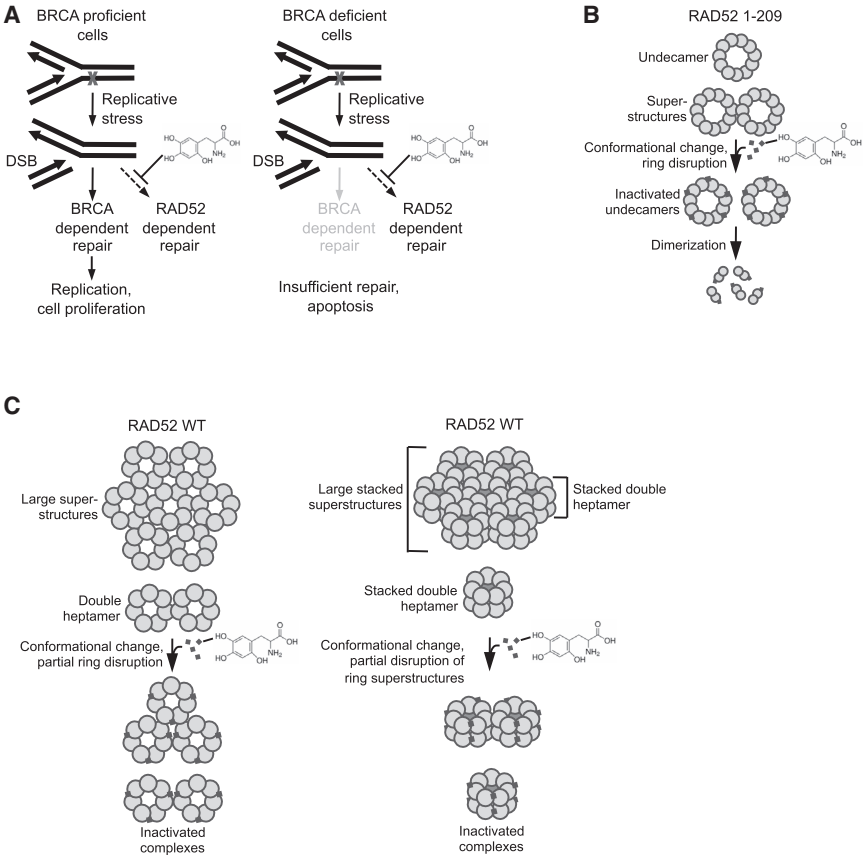

Figure 7. Models of Small-Molecule Inhibition of RAD52

(A) Models of 6-OH-dopa action. X = DNA damage.

(B) Model of small-molecule disruption of RAD52 undecamers.

(C) Models of small-molecule disruption of RAD52 WT heptamer superstructures (left) and stacked heptamer superstructures (right).

mechanism exhibited by 6-OH-dopa is clearly very specific. Small-molecule inhibition of Mre11 ssDNA binding by an allosteric mechanism has also been reported, demonstrating the success of this inhibitory method (Shibata et al., 2014).

Since our data suggest that five small molecules interact with the undecamer, we propose a model whereby one small molecule binds to every other subunit interface (Figure 7B). This scheme would account for approximately five small-molecule binding sites and provide a plausible mechanism by which 6-OH-dopa induces such a dramatic conformational change. For example, we propose that 6-OH-dopa binds to a region near the subunit interface that is critical for ring formation. This is supported by our data showing that the small molecule completely transforms undecamers into dimers when hydrophobic interactions are reduced by low salt. Such an interaction may induce a conformational change that inactivates ssDNA binding (Figure 7B). A total of five small-molecule binding events at alternating interfaces may then trigger dissociation of RAD52 rings into dimers (Figure 7B). In support of this model, previous studies suggest that particular residues involved in ssDNA binding also contribute to oligomerization or proper folding of the protein (Lloyd et al., 2005). Moreover, residues within the ssDNA binding domain promote self-association of RAD52 proteins in cells (Shen et al., 1996). Thus, 6-OH-dopa disruption of this region may also explain its ability to dissociate superstructures of the protein. A co-crystal structure of RAD52 1–209 bound to 6-OH-dopa is needed to identify the precise binding site.

Intriguingly, 6-OH-dopa exhibited a 31% lower IC_{50} for RAD52 WT (1.1 μM) compared with RAD52 1–209 (1.6 μM), indicating that fewer small molecules are required to inhibit the WT protein. Indeed, these data are consistent with the fact that RAD52 WT is composed of 36% fewer subunits than RAD52 1–209 and suggest that 36% fewer small molecules, for example approximately three, bind the heptamer, presumably at alternating subunit interfaces (Figure 7C, left). Since 6-OH-dopa precipitated RAD52 WT at high concentrations, we were unable to determine the number of binding sites by ITC.

Importantly, we found that 6-OH-dopa also altered the composition of RAD52 WT, which suggests that it induces a conformational change similar to that for RAD52 1–209. For example, 6-OH-dopa enabled RAD52 WT to enter a native gel as multiple discrete protein complexes in a manner similar to RAD52 1–209. Since a previous report claimed that large RAD52 heptamer ring superstructures prohibit RAD52 WT from entering gel filtration columns (Van Dyck et al., 1998), we examined whether the small molecule affected the gel filtration profile of RAD52 WT. Indeed, 6-OH-dopa enabled a significantly higher concentration of RAD52 WT to enter the column as superstructures and double heptamers. The small molecule, however, showed no evidence of dissociating heptamer rings into smaller complexes, which suggests that the C-terminal region of RAD52

(I) Plots showing viability of BRCA1-deficient MDA-MB-436 cells following transfection with scrambled (black) or RAD52 (white) siRNA and treatment with or without 6-OH-dopa. Data shown as average ± SEM from triplicates. *p = 0.0004, two-tailed Student's t test.

(J) Plots showing percent increase in γH2AX foci in BRCA1-proficient (black) and -deficient (gray) MDA-MB-436 cells following treatment with 6-OH-dopa (left). Percent increase was determined from the number of nuclei with greater than five γH2AX foci. Data shown as average ± SEM from three independent experiments. Cell images show DAPI staining (blue) and γH2AX foci (green) (right). **p = 0.002, ***p = 0.0078, two-tailed Student's t test.

(K) Plots showing percent of BRCA2-deficient (gray; VC8) and BRCA2-proficient (black; V79) cells positive for annexin V following treatment with 6-OH-dopa. *p = 0.01, **p = 0.003, two-tailed Student's t test (left). Plots showing percent of BRCA1-deficient (gray) and BRCA1-proficient (black) HCC1937 cells positive for annexin V following treatment with 6-OH-dopa (right).

WT contributes to ring formation or stability. Together, these data demonstrate that 6-OH-dopa disrupts large superstructures of RAD52 heptamer rings that are normally excluded from native gels and gel filtration columns (Figure 7C, left). Since a double heptamer was the smallest form of RAD52 WT detected by gel filtration, the possibility exists that RAD52 WT forms stacked double heptamers such as RAD51 (Figure 7C, right) (Shin et al., 2003). This modified model would explain why 6-OH-dopa is unable to fully disrupt these structures. Given that RAD52 superstructures and high-density RAD52 repair centers have been shown to promote DSB repair in vitro and in vivo (Lisby et al., 2001, 2003; Lloyd et al., 2002), respectively, and human RAD52 has been shown to self-associate in cells (Shen et al., 1996), the ability of the small molecule to disrupt heptamer ring superstructures likely contributes to its inhibitory effect in vivo.

Lastly, we demonstrated that 6-OH-dopa selectively halts the growth of a variety of BRCA-deficient cancer cells. For example, 6-OH-dopa treatment caused significant growth defects in *BRCA1*-mutated triple-negative breast cancer cell lines, but had little or no effect in the same cell lines complemented with WT *BRCA1*. Small-molecule growth inhibition of BRCA2-deficient cells, including the CAPAN-1 pancreatic cancer cell line, was also observed. Importantly, 6-OH-dopa also selectively halted the proliferation of BRCA-deficient AML and CML patient cells. Moreover, the small molecule caused a growth defect in these and other BRCA-deficient cells similar to that caused by olaparib, which was recently approved by the Food and Drug Administration. Hence, these data suggest that pharmacological inhibition of RAD52 may prove to be a successful alternative for treating BRCA-deficient cancers. Finally, we showed that 6-OH-dopa caused an increase in DNA damage and apoptosis in BRCA-deficient cells. Considering that RAD52 is heavily recruited to stalled replication forks (Figure 3A) (Lisby et al., 2001; Wray et al., 2008), our data support a model whereby 6-OH-dopa selectively kills BRCA-deficient cells by preventing RAD52 repair of DNA breaks caused by replication stress (Figure 7A).

In summary, our results demonstrate small-molecule disruption of RAD52 rings as a promising mechanism for precision medicine in BRCA-deficient cancers. Since RAD52 acts as a backup DNA repair factor in normal cells and RAD52 null mice show no major phenotypes, we anticipate that pharmacological inhibition of RAD52 in patients will enable selective killing of BRCA-deficient cancer cells while minimizing the risk of side effects in normal cells.

SIGNIFICANCE

Tumor suppressor proteins BRCA1 and BRCA2, which play major roles in HR and genome maintenance, are mutated in subsets of ovarian and breast cancers, and such inactivating BRCA mutations strongly predispose women to breast and ovarian cancer. Since BRCA-deficient cells are defective in HR, they are highly susceptible to drugs that cause DNA damage or suppress DNA repair. Therefore, BRCA-deficient cancers can be specifically targeted for killing via so-called precision medicines. Because suppression of the backup recombination factor RAD52 has been shown to cause synthetic lethality in BRCA-deficient cells, RAD52 is a promising drug target for precision medicine in HR-defective cancers. Here, we identify and characterize 6-OH-dopa as an effective small-molecule inhibitor of RAD52 in vitro and in cells. Unexpectedly, 6-OH-dopa acts via an allosteric mechanism, whereby it dimerizes undecamer rings of the RAD52 ssDNA binding domain whose activity is essential for the survival of BRCA-deficient cells. 6-OH-dopa also disrupts superstructures of full-length RAD52 heptamer rings, suppresses RAD52 foci formation at DNA damage, and selectively inhibits RAD52-mediated recombination in cells. Consistent with its ability to inhibit RAD52, 6-OH-dopa selectively kills BRCA-deficient cancer cells including those obtained from leukemia patients. These findings indicate that RAD52 is a "druggable" target, and suggest that small-molecule disruption of RAD52 rings may be an effective form of precision medicine for BRCA-deficient cancers.

EXPERIMENTAL PROCEDURES

Protein Purification

RAD52 WT

A histidine-tagged RAD52 WT expression vector (pFB581) (Benson et al., 1998) was transformed into Rosetta2(DE3)/pLysS cells (Stratagene). Freshly grown colonies were resuspended in 16 2.8-l Fernbach flasks each containing 1 l of LB broth supplemented with 100 μg/ml ampicillin and 34 μg/ml chloramphenicol. The flasks were shaken at room temperature until the optical density at 600 nm reached 0.5, then 0.8 mM isopropyl β-D-1-thiogalactopyranoside was added for an additional 4 hr. The biomass was then collected by centrifugation and stored at −80°C. Frozen pellets were thawed on ice and resuspended in lysis buffer (25 mM Tris-HCl [pH 7.5], 500 mM NaCl, 10% [v/v] glycerol, 10 mM imidazole [pH 8], 0.05% [v/v] NP-40 substitute [Thermo Scientific], 2 mM DTT, 10 mM PMSF, and Complete cocktail protease inhibitors [Roche]). Resuspended cells were sonicated on ice with constant stirring, then spun down twice at 35,000 rpm for 30 min at 4°C. The clarified cell lysate was loaded onto a 5-ml His-Trap column (GE Lifesciences), then washed in the following steps: 20 column volumes (CV) of lysis buffer, 10 CV of lysis buffer with 30 mM imidazole, 10 CV of lysis buffer with 60 mM imidazole, and 5 CV of lysis buffer with 80 mM imidazole. The bound protein was eluted in two steps with 200 and 500 mM imidazole, respectively, in buffer containing 25 mM Tris-HCl (pH 7.5), 500 mM NaCl, 10% (v/v) glycerol, 0.005% (v/v) NP-40 substitute, and 1 mM DTT. Fractions containing RAD52 were pooled, dialyzed against buffer A (25 mM Tris-HCl [pH 7.5], 75 mM NaCl, 10% glycerol, 1 mM DTT, and 0.001% NP-40), then loaded onto a 5-ml Q-Sepharose column and washed with the same buffer. The bound protein was then eluted in six steps of 1 CV each with buffer A containing increasing NaCl concentration as follows: 100, 125, 150, 200, 250, and 300 mM. Fractions containing pure RAD52 were dialyzed against storage buffer (25 mM Tris-HCl [pH 7.5], 100 mM NaCl, 10% glycerol, and 1 mM DTT). RAD52 WT was concentrated to 2.5 mg/ml and stored in aliquots at −80°C. All steps were performed at 4°C. RAD52 1–209 was purified as described (Singleton et al., 2002).

High-Throughput Screening

2 μl of 350 nM RAD52 WT was added to 384-well plates (Greiner Bio-One) containing 16 μl of buffer B (31.3 mM Tris-HCl [pH 7.5], 1.25 mM DTT, 31.3 mM NaCl, 0.013% NP-40, 0.63 mM $MgCl_2$, and 0.13 mg/ml BSA) and 18.75 μm of individual compounds from a highly diverse 18,304 small-molecule library and the Sigma Lopac collection. 2 μl of 100 nM FAM-conjugated ssDNA (RP316FAM) was then added and plates were centrifuged at 1,000 rpm for 30 s. After at least 30 min of incubation, FP was determined using a BioTek plate reader. High- and low-signal controls included and lacked RAD52, respectively. Reactions were performed at room temperature, and components were added using a Thermo MultiDrop Combi liquid handler.

IC_{50} Determination

40 nM RAD52 WT, 85 nM RAD52 1–209, 280 nM RAD51, or 300 nM RAD59 was mixed with reaction buffer C (25 mM Tris-HCl [pH 7.5], 1 mM DTT, 25 mM NaCl, 0.01% NP-40, 0.5 mM $MgCl_2$, and 0.1 mg/ml BSA), 10 nM FAM-conjugated ssDNA (RP316FAM), and indicated amounts of 6-OH-dopa in a total volume of 20 μl, then incubated at room temperature for 30 min. Reactions with RAD51 additionally contained 1 mM ATP. FP was then determined using a Clariostar (BMG Labtech) or BioTek plate reader. IC_{50} was determined by calculating the concentration of 6-OH-dopa required to inhibit ssDNA binding by 50% based on FP.

SUPPLEMENTAL INFORMATION

Supplemental Information includes Supplemental Experimental Procedures and six figures and can be found with this article online at http://dx.doi.org/10.1016/j.chembiol.2015.10.003.

AUTHOR CONTRIBUTIONS

G.C., S.M., K.S., and R.T.P. performed, designed, and interpreted experiments. T.K. purified RAD52 WT, assisted with light-scattering experiments, and provided conceptual and editorial input. A.L. was responsible for ITC experiments and analysis. M.A. performed light-scattering experiments and provided editorial input. S.M. purified RAD52 1–209 and eGFP-RAD52, and provided conceptual and editorial input. J.F.G. provided editorial input. T.S. provided conceptual input and was responsible for experiments with patient cells. R.T.P. conceived the study and wrote the manuscript.

ACKNOWLEDGMENTS

Research was funded by: Department of Defense (Breast Cancer Breakthrough Award W81XWH-14-1-0344), and in part by NIH (grant 1R01CA190237-01) and Temple University School of Medicine start-up funds to R.T.P., and NIH (grant 1R01CA186238) to T.S. We are grateful to M. Jacobson (Temple University School of Medicine) for use of the Clariostar (BMG Labtech) plate reader, S.C. West (Cancer Research UK) for RAD52 WT and 1–209 expression vectors, J. Stark (Beckman Research Institute City of Hope) for U2OS reporter cell lines, P. Sung (Yale University) for RAD51 expression vector, S. Powell (Memorial Sloan-Kettering Cancer Center) for eGFP-RAD52 expression vector, N. Johnson (Fox Chase Cancer Center) for MDA-MB-436 cells, and S.C. Kowalczykowski (University of California at Davis) for Rad59 protein.

Received: May 29, 2015
Revised: September 8, 2015
Accepted: October 4, 2015
Published: November 5, 2015

REFERENCES

Benson, F.E., Baumann, P., and West, S.C. (1998). Synergistic actions of Rad51 and Rad52 in recombination and DNA repair. Nature *391*, 401–404.

Ceccaldi, R., Liu, J.C., Amunugama, R., Hajdu, I., Primack, B., Petalcorin, M.I.R., O'Connor, K.W., Konstantinopoulos, P.A., Elledge, S.J., Boulton, S.J., et al. (2015). Homologous-recombination-deficient tumours are dependent on Polθ-mediated repair. Nature *518*, 258–262.

Chun, J., Buechelmaier, E.S., and Powell, S.N. (2013). Rad51 paralog complexes BCDX2 and CX3 act at different stages in the BRCA1-BRCA2-dependent homologous recombination pathway. Mol. Cell. Biol. *33*, 387–395.

Ciccia, A., and Elledge, S.J. (2010). The DNA damage response: making it safe to play with knives. Mol. Cell *40*, 179–204.

Cramer-Morales, K., Nieborowska-Skorska, M., Scheibner, K., Padget, M., Irvine, D.A., Sliwinski, T., Haas, K., Lee, J., Geng, H., Roy, D., et al. (2013). Personalized synthetic lethality induced by targeting RAD52 in leukemias identified by gene mutation and expression profile. Blood *122*, 1293–1304.

Deriano, L., and Roth, D.B. (2013). Modernizing the nonhomologous end-joining repertoire: alternative and classical NHEJ share the stage. Annu. Rev. Genet. *47*, 433–455.

Essers, J., Houtsmuller, A.B., van Veelen, L., Paulusma, C., Nigg, A.L., Pastink, A., Vermeulen, W., Hoeijmakers, J.H., and Kanaar, R. (2002). Nuclear dynamics of RAD52 group homologous recombination proteins in response to DNA damage. EMBO J. *21*, 2030–2037.

Farmer, H., McCabe, N., Lord, C.J., Tutt, A.N., Johnson, D.A., Richardson, T.B., Santarosa, M., Dillon, K.J., Hickson, I., Knights, C., et al. (2005). Targeting the DNA repair defect in BRCA mutant cells as a therapeutic strategy. Nature *434*, 917–921.

Feng, Z., Scott, S.P., Bussen, W., Sharma, G.G., Guo, G., Pandita, T.K., and Powell, S.N. (2011). Rad52 inactivation is synthetically lethal with BRCA2 deficiency. Proc. Natl. Acad. Sci. USA *108*, 686–691.

Francis, J.C., McCarthy, A., Thomsen, M.K., Ashworth, A., and Swain, A. (2010). Brca2 and Trp53 deficiency cooperate in the progression of mouse prostate tumourigenesis. PLoS Genet. *6*, e1000995.

Gibson, B.A., and Kraus, W.L. (2012). New insights into the molecular and cellular functions of poly(ADP-ribose) and PARPs. Nat. Rev. Mol. Cell Biol. *13*, 411–424.

Gunn, A., and Stark, J.M. (2012). I-SceI-based assays to examine distinct repair outcomes of mammalian chromosomal double strand breaks. Methods Mol. Biol. *920*, 379–391.

Gunn, A., Bennardo, N., Cheng, A., and Stark, J.M. (2011). Correct end use during end joining of multiple chromosomal double strand breaks is influenced by repair protein RAD50, DNA-dependent protein kinase DNA-PKcs, and transcription context. J. Biol. Chem. *286*, 42470–42482.

Ji, Y., and Tulin, A.V. (2010). The roles of PARP1 in gene control and cell differentiation. Curr. Opin. Genet. Dev. *20*, 512–518.

Kagawa, W., Kurumizaka, H., Ishitani, R., Fukai, S., Nureki, O., Shibata, T., and Yokoyama, S. (2002). Crystal structure of the homologous-pairing domain from the human Rad52 recombinase in the undecameric form. Mol. Cell *10*, 359–371.

Kaufman, B., Shapira-Frommer, R., Schmutzler, R.K., Audeh, M.W., Friedlander, M., Balmana, J., Mitchell, G., Fried, G., Stemmer, S.M., Hubert, A., et al. (2015). Olaparib monotherapy in patients with advanced cancer and a germline BRCA1/2 mutation. J. Clin. Oncol. *33*, 244–250.

Krogh, B.O., and Symington, L.S. (2004). Recombination proteins in yeast. Annu. Rev. Genet. *38*, 233–271.

Li, X., and Heyer, W.D. (2008). Homologous recombination in DNA repair and DNA damage tolerance. Cell Res. *18*, 99–113.

Lisby, M., Rothstein, R., and Mortensen, U.H. (2001). Rad52 forms DNA repair and recombination centers during S phase. Proc. Natl. Acad. Sci. USA *98*, 8276–8282.

Lisby, M., Mortensen, U.H., and Rothstein, R. (2003). Colocalization of multiple DNA double-strand breaks at a single Rad52 repair centre. Nat. Cell Biol. *5*, 572–577.

Liu, J., and Heyer, W.D. (2011). Who's who in human recombination: BRCA2 and RAD52. Proc. Natl. Acad. Sci. USA *108*, 441–442.

Lloyd, J.A., Forget, A.L., and Knight, K.L. (2002). Correlation of biochemical properties with the oligomeric state of human rad52 protein. J. Biol. Chem. *277*, 46172–46178.

Lloyd, J.A., McGrew, D.A., and Knight, K.L. (2005). Identification of residues important for DNA binding in the full-length human Rad52 protein. J. Mol. Biol. *345*, 239–249.

Lok, B.H., and Powell, S.N. (2012). Molecular pathways: understanding the role of Rad52 in homologous recombination for therapeutic advancement. Clin. Cancer Res. *18*, 6400–6406.

Lok, B.H., Carley, A.C., Tchang, B., and Powell, S.N. (2013). RAD52 inactivation is synthetically lethal with deficiencies in BRCA1 and PALB2 in addition to BRCA2 through RAD51-mediated homologous recombination. Oncogene *32*, 3552–3558.

Lord, C.J., and Ashworth, A. (2012). The DNA damage response and cancer therapy. Nature *481*, 287–294.

Mai, P.L., Chatterjee, N., Hartge, P., Tucker, M., Brody, L., Struewing, J.P., and Wacholder, S. (2009). Potential excess mortality in BRCA1/2 mutation carriers

beyond breast, ovarian, prostate, and pancreatic cancers, and melanoma. PLoS One *4*, e4812.

McCabe, N., Turner, N.C., Lord, C.J., Kluzek, K., Bialkowska, A., Swift, S., Giavara, S., O'Connor, M.J., Tutt, A.N., Zdzienicka, M.Z., et al. (2006). Deficiency in the repair of DNA damage by homologous recombination and sensitivity to poly(ADP-ribose) polymerase inhibition. Cancer Res. *66*, 8109–8115.

Moynahan, M.E., and Jasin, M. (2010). Mitotic homologous recombination maintains genomic stability and suppresses tumorigenesis. Nat. Rev. Mol. Cell Biol. *11*, 196–207.

Patel, S.S., and Picha, K.M. (2000). Structure and function of hexameric helicases. Annu. Rev. Biochem. *69*, 651–697.

Petukhova, G., Stratton, S.A., and Sung, P. (1999). Single strand DNA binding and annealing activities in the yeast recombination factor Rad59. J. Biol. Chem. *274*, 33839–33842.

Podszywalow-Bartnicka, P., Wolczyk, M., Kusio-Kobialka, M., Wolanin, K., Skowronek, K., Nieborowska-Skorska, M., Dasgupta, Y., Skorski, T., and Piwocka, K. (2014). Downregulation of BRCA1 protein in BCR-ABL1 leukemia cells depends on stress-triggered TIAR-mediated suppression of translation. Cell Cycle *13*, 3727–3741.

Rijkers, T., Van Den Ouweland, J., Morolli, B., Rolink, A.G., Baarends, W.M., Van Sloun, P.P., Lohman, P.H., and Pastink, A. (1998). Targeted inactivation of mouse RAD52 reduces homologous recombination but not resistance to ionizing radiation. Mol. Cell. Biol. *18*, 6423–6429.

Scheuermann, T.H., Li, Q., Ma, H.W., Key, J., Zhang, L., Chen, R., Garcia, J.A., Naidoo, J., Longgood, J., Frantz, D.E., et al. (2013). Allosteric inhibition of hypoxia inducible factor-2 with small molecules. Nat. Chem. Biol. *9*, 271–276.

Shen, Z., Peterson, S.R., Comeaux, J.C., Zastrow, D., Moyzis, R.K., Bradbury, E.M., and Chen, D.J. (1996). Self-association of human RAD52 protein. Mutat. Res. *364*, 81–89.

Shibata, A., Moiani, D., Arvai, A.S., Perry, J., Harding, S.M., Genois, M.M., Maity, R., van Rossum-Fikkert, S., Kertokalio, A., Romoli, F., et al. (2014). DNA double-strand break repair pathway choice is directed by distinct MRE11 nuclease activities. Mol. Cell *53*, 7–18.

Shin, D.S., Pellegrini, L., Daniels, D.S., Yelent, B., Craig, L., Bates, D., Yu, D.S., Shivji, M.K., Hitomi, C., Arvai, A.S., et al. (2003). Full-length archaeal Rad51 structure and mutants: mechanisms for RAD51 assembly and control by BRCA2. EMBO J. *22*, 4566–4576.

Singleton, M.R., Wentzell, L.M., Liu, Y., West, S.C., and Wigley, D.B. (2002). Structure of the single-strand annealing domain of human RAD52 protein. Proc. Natl. Acad. Sci. USA *99*, 13492–13497.

Stark, J.M., Pierce, A.J., Oh, J., Pastink, A., and Jasin, M. (2004). Genetic steps of mammalian homologous repair with distinct mutagenic consequences. Mol. Cell. Biol. *24*, 9305–9316.

Stasiak, A.Z., Larquet, E., Stasiak, A., Muller, S., Engel, A., Van Dyck, E., West, S.C., and Egelman, E.H. (2000). The human Rad52 protein exists as a heptameric ring. Curr. Biol. *10*, 337–340.

Sung, P., and Klein, H. (2006). Mechanism of homologous recombination: mediators and helicases take on regulatory functions. Nat. Rev. Mol. Cell Biol. *7*, 739–750.

Thomas, C., and Tulin, A.V. (2013). Poly-ADP-ribose polymerase: machinery for nuclear processes. Mol. Aspects Med. *34*, 1124–1137.

Turner, N., Tutt, A., and Ashworth, A. (2004). Hallmarks of 'BRCAness' in sporadic cancers. Nat. Rev. Cancer *4*, 814–819.

Tutt, A., Bertwistle, D., Valentine, J., Gabriel, A., Swift, S., Ross, G., Griffin, C., Thacker, J., and Ashworth, A. (2001). Mutation in Brca2 stimulates error-prone homology-directed repair of DNA double-strand breaks occurring between repeated sequences. EMBO J. *20*, 4704–4716.

Van Dyck, E., Hajibagheri, N.M., Stasiak, A., and West, S.C. (1998). Visualisation of human rad52 protein and its complexes with hRad51 and DNA. J. Mol. Biol. *284*, 1027–1038.

Van Dyck, E., Stasiak, A.Z., Stasiak, A., and West, S.C. (2001). Visualization of recombination intermediates produced by RAD52-mediated single-strand annealing. EMBO Rep. *2*, 905–909.

Wang, Y., McKay, J.D., Rafnar, T., Wang, Z., Timofeeva, M.N., Broderick, P., Zong, X., Laplana, M., Wei, Y., Han, Y., et al. (2014). Rare variants of large effect in BRCA2 and CHEK2 affect risk of lung cancer. Nat. Genet. *46*, 736–741.

Wray, J., Liu, J., Nickoloff, J.A., and Shen, Z. (2008). Distinct RAD51 associations with RAD52 and BCCIP in response to DNA damage and replication stress. Cancer Res. *68*, 2699–2707.

Wu, Y., Sugiyama, T., and Kowalczykowski, S.C. (2006). DNA annealing mediated by Rad52 and Rad59 proteins. J. Biol. Chem. *281*, 15441–15449.

Yu, X., and Egelman, E.H. (1997). The RecA hexamer is a structural homologue of ring helicases. Nat. Struct. Biol. *4*, 101–104.

